Biophysical Journal, Volume *116*

Supplemental Information

Probe Sensitivity to Cortical versus Intracellular Cytoskeletal Network Stiffness

Amir Vahabikashi, Chan Young Park, Kristin Perkumas, Zhiguo Zhang, Emily K. Deurloo, Huayin Wu, David A. Weitz, W. Daniel Stamer, Robert D. Goldman, Jeffrey J. Fredberg, and Mark Johnson

SUPPLEMENTAL INFORMATION

AFM measurements. To determine the aggregate cell modulus (E) for a rounded AFM tips of radius R, we used the following relationship (1):

$$E = \frac{3\,F\,(1-\upsilon^2)}{4\,R^{1/2}\delta^{3/2}} \tag{S1}$$

where F is the applied force, δ is the indentation, and ν=0.5 is Poisson ratio (2-4). For sharp tips, we used a model for pyramidal indenters that accounts for the spherical cap at the apex of the AFM tip (5, 6):

$$F = \frac{2E}{(1-\upsilon^2)}\left\{a\delta - \frac{\sqrt{2}\,a^2}{\pi\,tan\theta}\left[\frac{\pi}{2} - sin^{-1}\left(\frac{b}{a}\right)\right] - \frac{a^3}{3R} + (a^2-b^2)^{1/2}\left[\frac{\sqrt{2}\,b}{\pi\,tan\theta} + \frac{(a^2-b^2)}{3R}\right]\right\} \tag{S2a}$$

$$\delta + \frac{a}{R}\left[a - (a^2-b^2)^{1/2}\right] + \frac{2\sqrt{2}\,a}{\pi\,tan\theta}\left[\frac{\pi}{2} - sin^{-1}\left(\frac{b}{a}\right)\right] = 0 \tag{S2b}$$

where $b=R\cos\theta$ *(θ=20°),* and *R* is the radius of the spherical cap (20 nm). Equation (S2b) is used to find the effective radius of contact *a* for any indentation δ, and then used in equation (S2a) to find *E*, for a given force *F*. We have previously shown that this model gives value of *E* that are relatively independent of δ for value of δ greater than approximately 100 nm (7).

Fig. S1 shows typical force-ramp AFM curves and their corresponding fits from equations (S2) or (S1) for sharp (A, C) and rounded (B, D) AFM tips, respectively. The fits are found by determining the average modulus that best fits the data for $\delta \gtrsim 100$ nm and then using that modulus in equation (S1) or (S2). The particular examples shown compare results for (i) control and α-actinin overexpressing SC cells for a sharp (A) and a round tip (B), respectively, and (ii) wild-type and vimentin-KO MEFs for a sharp tip (C) and a round tip (D), respectively.

Results from individual SC cell strains. Fig. S11 shows additional image of filamentous actin (F-actin) and phosphorylated myosin light chain (P-myosin) in confluent SC cells treated with dexamethasone (1μM) as compared with controls. Fig. S2 shows the results from individuals SC cells

strains treated with dexamethasone and then measured with AFM sharp-tip (A), AFM round-tip (B), TM (C), and OMTC (D). Fig. S3 shows the results from individuals SC cells strains transduced with GFP, α-actinin or RhoA and then measured with AFM sharp-tip (A), AFM round-tip (B), TM (C), and OMTC (D).

Additional results from finite element modeling. Fig. S4 and S5 show the strain and stress distributions for the same cases considered in Fig. 6, that shows the strain energy distribution. For AFM sharp-tips, strain was localized around sharp tip within cortical network and did not propagate through intracellular network (Fig S4 A, B). The smallest AFM round-tips considered (diameter of 0.8 μm) show the strain propagated into intracellular network and the presence of a stiff cortex (E_{cortex} = 50*$E_{intracellular}$) increased the distance to which strain propagated (Fig S4 C, D). This trend is continued for largest AFM round tip considered (10 μm) with the strain now extending throughout the intracellular network (Fig S4 E, F). The stress fields (Figure S5) show similar trends, but show considerable stress within the cortex in all cases.

For OMTC, the strain propagated through intracellular network but the stiff cortex increased the propagation distance significantly (Fig S4 G-H). In contrast to strain distribution, the stiff cortex lead to a stress distribution localized close to cortical layer in all conditions (Fig S5).

We examined the effect that cell thickness would have on our results. We examined cells with E_{cortex}=50*$E_{intracellular}$, varying cell thickness from 2.75-30 μm. We found that for cells thicker than approximately 5 μm, there was little effect on $E_{apparent}$ (inset in Fig. 6B) and a minimal effect on strain energy distribution as shown in Fig. S6. Similar studies were done modeling the effect of cell thickness on an AFM 10 μm tip measurements of $E_{apparent}$ with the results shown in Fig. S9.

One peculiar result in the OMTC studies is that a monotonic relationship was not found between $E_{apparent}$ and bead embedding depth (see Fig. 7B). Fig. S7 shows this result in more detail for the case of E_{cortex}=50*$E_{intracellular}$. This result arises because of several competing effects. First, if we consider

only the effects of the cortex surrounding the bead and an unbounded cell below, then it would be expected that as the bead is embedded more deeply (thus increasing the radius of the contact area, then $E_{apparent}$ should approach $E_{intracellular}$ (8). However, two effects counter this. First, as the bead is embedded more deeply, the substrate increasingly influences $E_{apparent}$ because of the finite cell thickness (see insert in Fig. 7B). Also, the distal cortex (the part of the cortex that does not directly surround the bead) shows an increased concentration of strain energy for deeply embedded beads (Fig. S8). Both of these effects act to increase $E_{apparent}$ and thereby explain the non-montonic behavior shown in Figs. 6B and S7.

Mijailovic et al. (9) defined a function β that used to determine how the effective shear modulus was affected by embedding depth. Fig. S10 shows a comparison of our calculated values of β as compared to the values from Mijailovic et al. (9) for the case when $E_{cortex} = E_{intracellular}$ showing good agreement with the differences presumably due to differences in the discretization used to create the finite element mesh. We extended this same definition of β (see methods) for a non-homogenous case, E_{cortex}=50* $E_{intracellular}$, the results of which are also shown in Fig. S10.

Statistical techniques used. All statistical analyses were done using JMP Pro 13.0.0. Measurements of cell mechanical properties (geometric means) following dexamethasone treatment were fit with "Fit Model: Standard Least Square" as a function of dexamethasone concentration; the "Center Polynomials" option was not chosen. The results for the three curves fits shown in Figures 2A and 2B are as follows:

AFM sharp tip: $E = 10.43 + 8.53 * [DEX]$

TM: $T = 35.0 + 11.07 * [DEX]$

OMTC $g' = 0.58 - 0.176 * [DEX]$

where E is modulus (kPa), T is RMS traction (Pa), g' is the apparent shear modulus (Pa/nm) and [DEX] is the dexamethasone concentration (μM).

Difference of measurements of cell mechanical properties following induction of GFP, α-actinin, or RhoA were analyzed with "Fit Model: Mixed Model" using the Multiple Comparison option, comparing all pairs with a Tukey correction. In all of these cases, cell strain was included as a random effect attribute to account for within strain variability. Differences of cell mechanical properties between wildtype and knockout MEFS were analyzed with a "t-test" under "Fit Y by X".

REFERENCES

1. Harding, J. W., and I. N. Sneddon. 1945. The elastic stresses produced by the indentation of a plane surface of a semi-infinite elastic solid by a rigid punch. Mathematical Proceedings of the Cambridge Philosophical Society 41:16-26.
2. Harris, A. R., and G. T. Charras. 2011. Experimental validation of atomic force microscopy-based cell elasticity measurements. Nanotechnology 22(34):345102-345101 to 345102-345110.
3. Sirghi, L., J. Ponti, F. Broggi, and F. Rossi. 2008. Probing elasticity and adhesion of live cells by atomic force microscopy indentation. European Biophysics Journal with Biophysics Letters 37(6):935-945.
4. Costa, K. D. 2003. Single-cell elastography: Probing for disease with the atomic force microscope. Disease Markers 19(2-3):139-154.
5. Rico, F., P. Roca-Cusachs, N. Gavara, R. Farre, M. Rotger, and D. Navajas. 2005. Probing mechanical properties of living cells by atomic force microscopy with blunted pyramidal cantilever tips. Physical Review E 72(2):021914-021911 to 021914-021910.
6. Lin, D. C., E. K. Dimitriadis, and F. Horkay. 2007. Robust strategies for automated AFM force curve analysis--I. Non-adhesive indentation of soft, inhomogeneous materials. Journal of Biomechanical Engineering 129(3):430-440.
7. Vargas-Pinto, R., H. Gong, A. Vahabikashi, and M. Johnson. 2013. The effect of the endothelial cell cortex on atomic force microscopy measurements. Biophysical Journal 105(2):300-309.
8. Tracqui, P., and J. Ohayon. 2007. Rotational microrheology of multilayered finite elastic media. Journal of Applied Physics 102(3):033517.
9. Mijailovich, S. M., M. Kojic, M. Zivkovic, B. Fabry, and J. J. Fredberg. 2002. A finite element model of cell deformation during magnetic bead twisting. Journal of Applied Physiology 93(4):1429-1436.

FIGURES

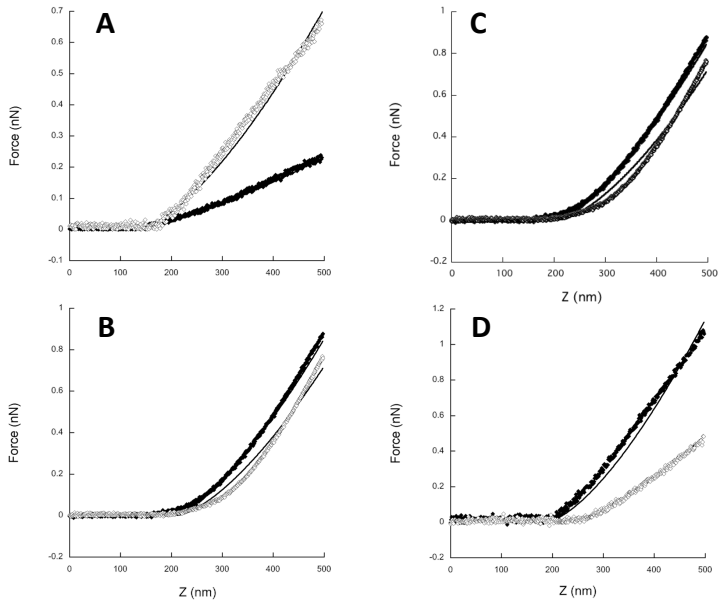

Fig. S1: Typical force curves for AFM sharp (panels A, C) and round tips (panels B, D) as a function of ramp distance (Z). Panels A and B compare α-actinin over-expressing SC cells (open symbols) with control SC cells (closed symbols), while Panels C and D compare wild-type MEFs (closed symbols) with vimentin-KO MEFs (open symbols). Fits (solid lines) are from equations (S1: B, D) or (S2: A, C); if line is not visible, it is under the data points.

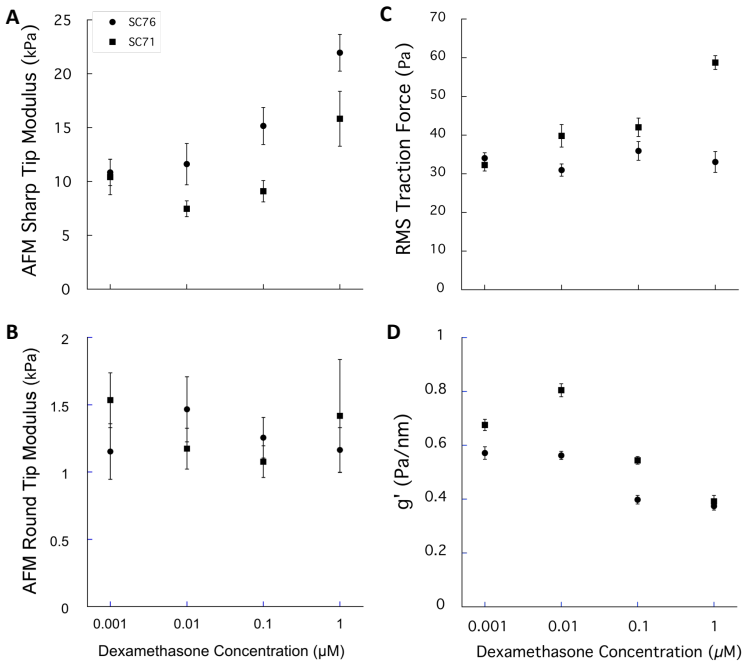

Fig. S2: Measurements of cell biophysical properties of confluent SC cells after treatment with varying concentrations of dexamethasone. (A) Sharp AFM tip; (B) Round AFM Tip; (C) TM; (D) OMTC. Geometric Mean ± S.E. about geometric means.

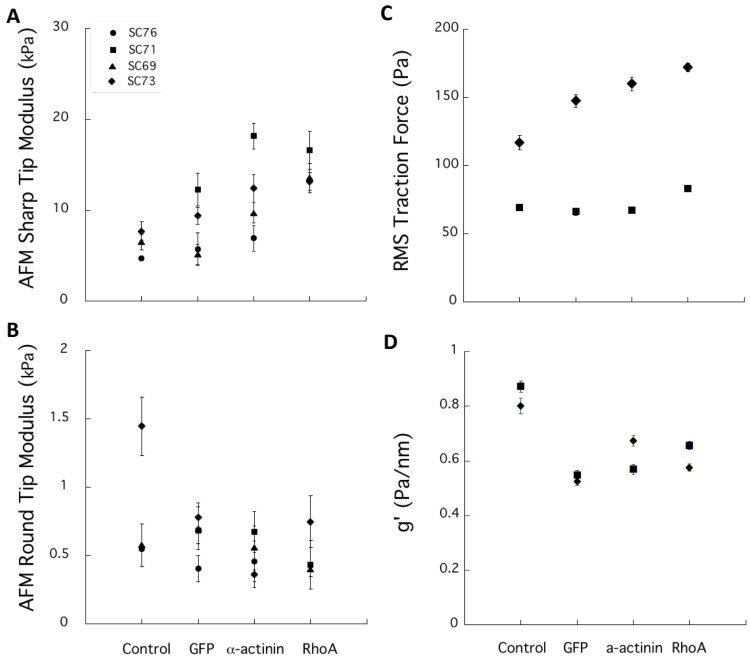

Fig. S3: Measurements of cell biophysical properties of subconfluent SC cells after being transduced with GFP, α-actinin or RhoA, as compared with control. (A) Sharp AFM tip; (B) Round AFM Tip; (C) TM; (D) OMTC. Geometric Mean ± S.E. about geometric means.

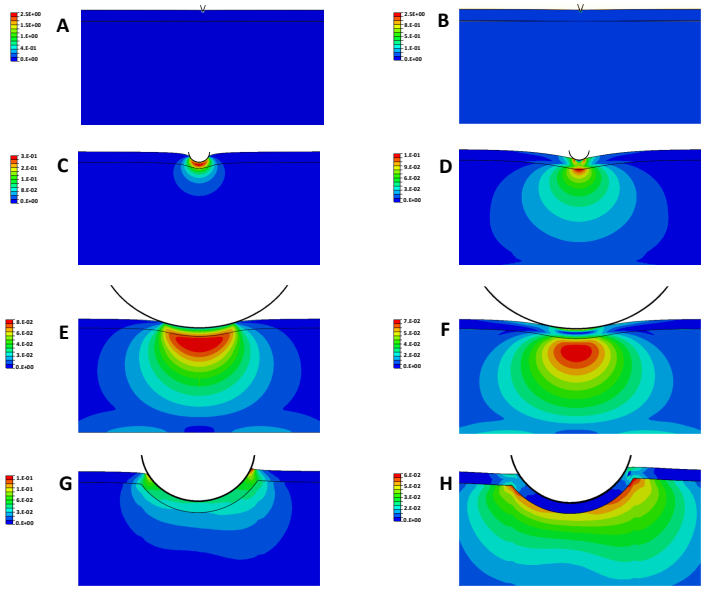

Fig. S4: Strain distribution (logarithmic strain) for indentation into a cell of a sharp AFM tip (A,B), a 0.8 µm diameter rounded AFM tip (C, D), a 10 µm diameter rounded AFM tip (E, F) and a 4.5 µm OMTC bead (G, H). The OMTC bead is embedded 25% of its diameter into the cell and twisted by a torque of 60 Pa applied in a counter-clockwise fashion. Panels A, C, E, G are for cases with E_{cortex}=$E_{intracellular}$; panels B, D, F, H are for E_{cortex}=50*$E_{intracellular}$. Cell thickness is 5 µm. $E_{intracelluar}$ = 1 kPa for AFM model (7) and 3 kPa for OMTC model (9).

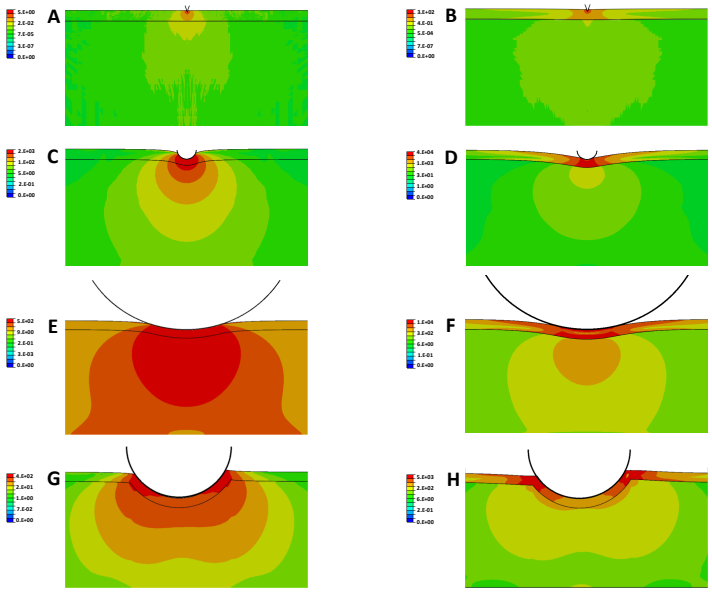

Fig. S5: Stress distribution (log scale, Pa) for indentation into a cell of a sharp AFM tip (A,B), a 0.8 µm diameter rounded AFM tip (C, D), a 10 µm diameter rounded AFM tip (E, F) and a 4.5 µm OMTC bead (G,H). The OMTC bead is embedded 25% of its diameter into the cell and twisted by a torque of 60 Pa applied in a counter-clockwise fashion. Panels A, C, E, G are for cases with $E_{cortex}=E_{intracellular}$; panels B, D, F, H are for $E_{cortex}=50*E_{intracellular}$. Cell thickness is 5 µm. $E_{intracelluar}$ = 1 kPa for AFM model (7) and 3 kPa for OMTC model (9)

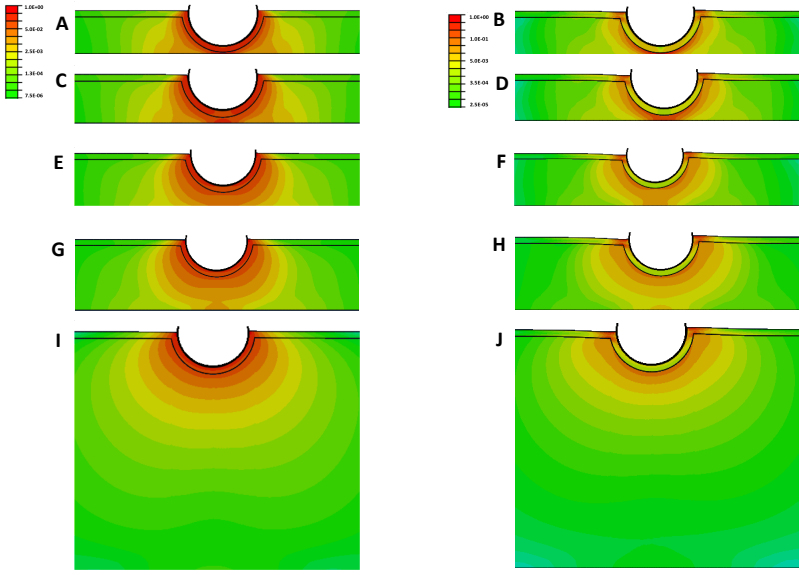

Fig. S6: Strain energy density distribution (log scale) for the twisting of a 4.5 µm OMTC bead into cells with $E_{cortex}=E_{intracellular}$ (A, C, E, G, I) or $E_{cortex}=50*E_{intracellular}$ (B, D, F, H, J) for cell thicknesses of 2.75 µm (A, B), 3.17 µm (C, D), 4.2 µm (E, F), 5 µm (G, H) and 15 µm (I, J). The strain energy distribution in each panel is normalized to the maximum strain energy in that panel and a log scale is used.

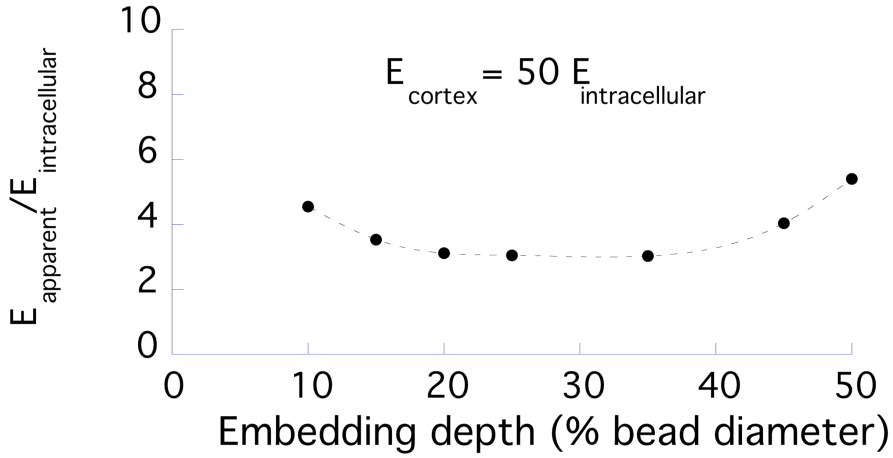

Fig. S7: $E_{apparent}/E_{intracellular}$ as a function of OMTC bead embedding depth with $E_{cortex}/E_{intracellular}$=50. Cell thickness is 5 μm.

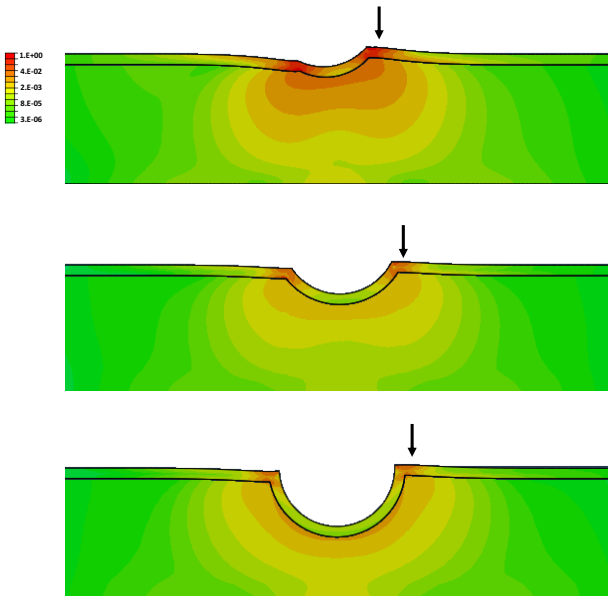

Fig. S8: Strain energy distribution (log scale) for the twisting of a 4.5 µm OMTC bead into cells with E_{cortex}=50*$E_{intracellular}$ for embedding depths of (A) 10%, (B), 25% and (C) 50%. Arrows point to high strain energy densities in distal cortex. Cell thickness is 5 µm. The strain energy distribution in each panel is normalized to the maximum strain energy in that panel and a log scale is used.

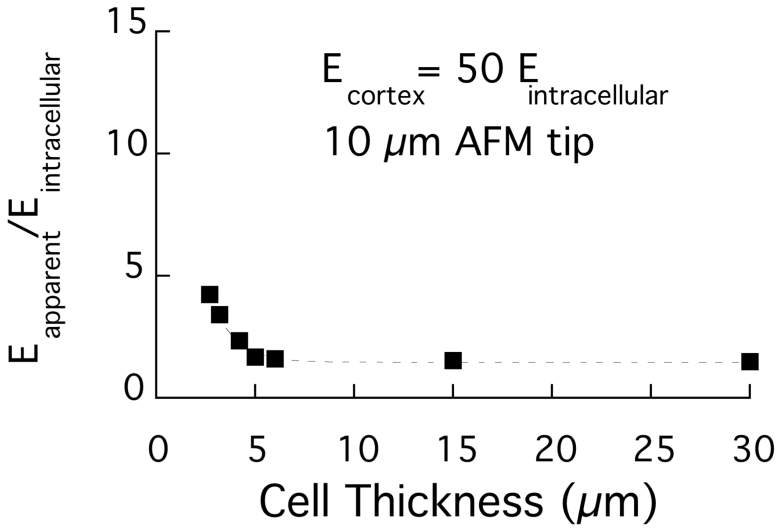

Fig. S9: Results for a 10 μm AFM probe indenting 400 nm into a cell with $E_{cortex}/E_{intracellular}$=50 for cell thicknesses ranging from 2.75-30 μm.

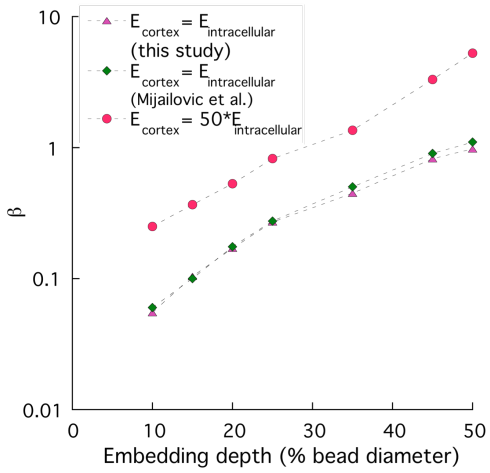

Fig. S10: Function β defined by Mijailovic et al. (9) for cell of thickness of 5 μm for case where $E_{cortex}=E_{intracellular}$ for this study as compared to the results of Mijailovic et al., and for the case where $E_{cortex}=50*E_{intracellular}$.

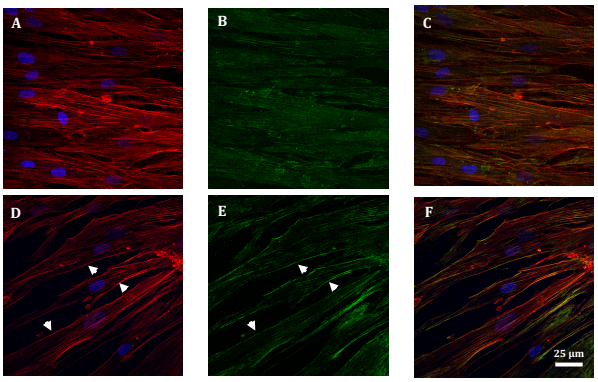

Fig. S11: Additional confocal images of confluent monolayer of SC cells treated with vehicle (A-C) and 1µM dexamethasone (D-F); F-actin (red, A & D), phosphorylated myosin (green, B & E), nucleus (blue) and overlaid (C & F). Stress fibers are seen in both groups but the stress fibers are prominent on cortex regions in dexamethasone treated cells (white arrows in D). Also, while p-myosin is present in both groups, it is more concentrated at the cortex of dexamethasone-treated cells (white arrows in E).